

Asymmetric shifts in precipitation due to urbanization across global cities

Received: 10 January 2025

Accepted: 12 June 2025

Published online: 01 July 2025

Jinghua Xiong^{1,2}, Yuting Yang^{1,2}✉, Long Yang³ & Dawen Yang^{1,2}✉

Urbanization alters precipitation patterns by modifying thermal, dynamic, and chemical processes in the atmosphere. However, its effect on precipitation regimes, particularly at the sub-daily scale, is poorly understood. In this work, we use a high-resolution, spatially continuous satellite precipitation dataset to examine urbanization-induced shifts across precipitation intensities over global cities. We show that urbanization generally causes asymmetric shifts, increasing lower-intensity events and decreasing higher-intensity ones, with distinct patterns in tropical monsoon regions. These shifts, primarily driven by changes in event frequency, lead to reduced precipitation variability in urban areas, particularly in temperate cities and those exhibiting higher urbanization levels. Sub-daily analysis reveals that lower-intensity precipitation most notably increases in the early morning, while higher-intensity events decrease in the late afternoon, dampening diurnal precipitation variability. These findings offer important observational evidence of how urbanization alters precipitation regimes and highlight the need for adaptive urban water management strategies.

Cities, which now accommodate ~55% of the global population, have expanded threefold over the past three decades¹. While urbanization has driven economic growth and social progress, it has also introduced profound environmental disruptions, altering urban climates and exacerbating climate-related hazards². Urban climate phenomena, such as urban heat islands (UHIs) and urban dry or wet islands, are well-documented, characterized by elevated temperatures and altered humidity compared to surrounding rural areas^{3,4}. However, the impact of urbanization on regional precipitation regimes remains poorly understood due to the complex interplay of factors such as city-specific attributes, climatic conditions, and limited data availability⁵. This knowledge gap is particularly pronounced for sub-daily precipitation, which plays a critical role in urban hydrological hazards, including flash floods.

Urbanization influences precipitation through multiple interconnected mechanisms. Anthropogenic heat emissions and increased surface roughness enhance convective processes^{6,7}, while land-use changes influence regional moisture supply by altering evaporation

patterns³. Urban structures disrupt wind fields and moisture transport⁸, and anthropogenic aerosols modulate precipitation by serving as cloud condensation nuclei or influencing atmospheric heating and cooling^{9,10}. These mechanisms operate at diverse spatial and temporal scales, exhibiting variability depending on the time of day and background environmental conditions¹¹. Existing evidence generally suggests that urbanization increases total precipitation in many global cities, particularly in coastal and tropical regions¹². However, changes in extreme precipitation are more heterogeneous^{13–18}, often exhibiting city-specific and region-dependent characteristics. Despite these insights, a comprehensive global synthesis of urbanization's impact on precipitation remains lacking. Notably, previous research has largely concentrated on total and extreme precipitation metrics, with limited attention to how urbanization affects the full distribution of precipitation intensities—particularly on a global scale^{5,11,19–21}. This knowledge gap is critical, as shifts across different precipitation intensities have distinct implications for urban planning, stormwater management, and climate adaptation strategies^{22,23}.

¹State Key Laboratory of Hydrosience and Engineering, Tsinghua University, Beijing, China. ²Department of Hydraulic Engineering, Tsinghua University, Beijing, China. ³School of Geography and Ocean Science, Nanjing University, Nanjing, Jiangsu Province, China. ✉e-mail: Yuting_Yang@tsinghua.edu.cn; yangdw@tsinghua.edu.cn

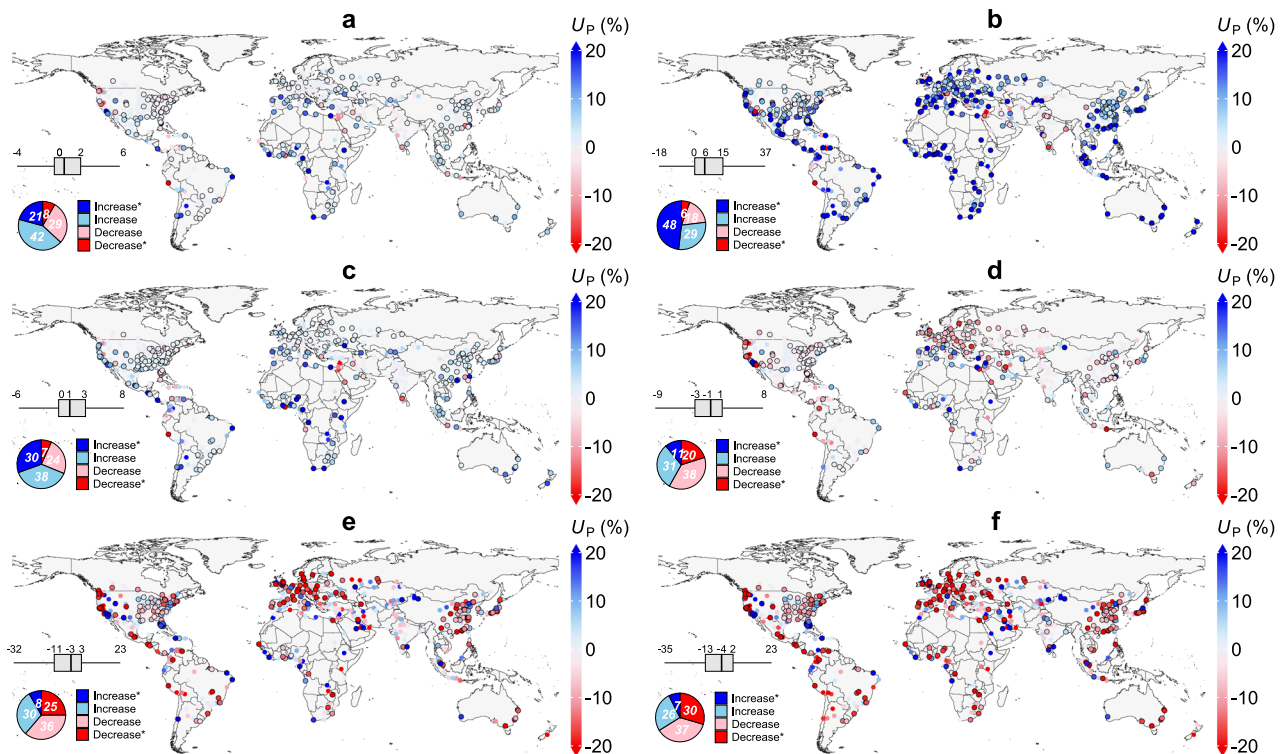


Fig. 1 | Climatology of urbanization effects on precipitation (2001–2023). **a–e** Spatial distribution of urbanization effects (U_P , %) on total, drizzle, light, moderate, and heavy precipitation across 741 cities. **f** Spatial distribution of urbanization effects on the heavy-to-light precipitation ratio (HLP). Urbanization effects are quantified as the precipitation difference between urban areas and their surrounding rural counterparts (see “Methods”). Cities outlined in black indicate

statistically significant differences. Pie charts illustrate the proportion of cities exhibiting varying urbanization effects, while the boxplot summarizes the statistical distribution of these effects. The box represents the interquartile range (25th–75th percentiles), and whiskers denote the minimum and maximum values excluding outliers. Source data are provided as a Source Data file.

Furthermore, previous research has predominantly analyzed daily (for extreme precipitation) or longer (for both total and extreme precipitation) timescales, leaving diurnal variations in urbanization-induced precipitation changes underexplored. While a few regional studies have investigated super city clusters^{24–27}, global-scale assessments of sub-daily precipitation responses to urbanization remain scarce.

To address these important knowledge gaps, here we employ hourly satellite-based precipitation data and a paired approach to examine the impacts of urbanization on precipitation across global cities (see “Methods”). Unlike previous studies that predominantly analyzed daily or longer timescales, our approach leverages hourly data to provide a detailed characterization of precipitation across varying intensity levels, including drizzle (0.1–0.5 mm/h), light (0.5–2.5 mm/h), moderate (2.5–10 mm/h), and heavy (≥ 10 mm/h), along with their diurnal patterns. By analyzing climatological contrasts from 2001 to 2023, we identify urbanization-induced shifts in precipitation characteristics. This global-scale assessment advances our understanding of urban hydro-climatic dynamics and offers valuable insights for developing adaptive strategies to mitigate water-related hazards in urban regions.

Results

Urbanization effects on precipitation regimes

We first examined urbanization-induced changes in total precipitation over the period 2001–2023 (Fig. 1a). Our findings reveal that 63% of global cities experienced an increase in total precipitation, nearly twice the proportion of cities showing a decrease (37%). Precipitation increases were most prominent in coastal cities across Africa, Asia/Oceania, and North America, with Yaoundé, Cameroon, exhibiting the

highest increase (+64%). When considering statistical significance, approximately one-fifth of the cities (21%) showed significant increases in total precipitation amount attributed to urbanization, compared to 8% exhibiting significant decreases. Further analysis revealed a significant decline in precipitation amounts with increasing distance from city centers, reinforcing the link between urbanization and enhanced precipitation (Supplementary Fig. 1).

Next, we investigated how urbanization affects precipitation across different intensity levels. The analysis reveals a clear trend: urbanization tends to increase the accumulation of lower-intensity precipitation while suppressing higher-intensity events. Specifically, drizzle and light precipitation amounts increased in 77% and 68% of cities, respectively, whereas moderate and heavy precipitation increased in only 42% and 38% of cities (Fig. 1b–e). On average, drizzle and light precipitation amounts in urban areas were 6% and 1% higher, respectively, than in rural counterparts. In contrast, moderate and heavy precipitation were 1% and 3% lower, respectively.

To quantify these asymmetric changes, we introduced the heavy-to-light precipitation (HLP) ratio as a metric to capture the distributional shifts in precipitation (see “Methods”). As can be expected from the above findings, a widespread reduction in HLP occurred in most cities (67%) across all major continents, reflecting a more balanced precipitation distribution associated with urbanization. Only 33% of cities, predominantly in coastal regions of the southern United States, the Arabian Peninsula, and western Africa, showed increases in HLP (Fig. 1f). Seasonal analyses revealed that the asymmetric nature of urbanization-induced precipitation changes persists across all seasons, albeit with notable regional and magnitude differences (Supplementary Figs. 2–5). For example, winter exhibited the most substantial mean increase in total precipitation (23%), driven primarily

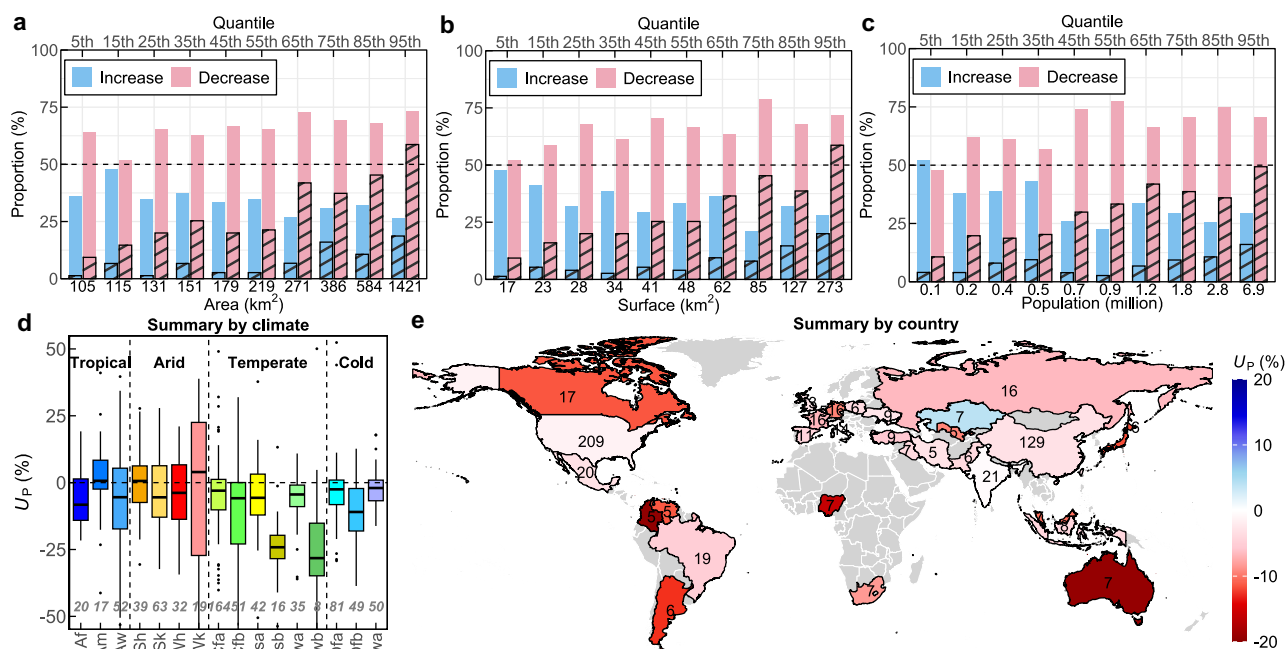


Fig. 2 | Characteristics of urbanization effects on precipitation. **a–c** Proportion of cities exhibiting varying urbanization effects on the heavy-to-light precipitation ratio (HLP) with respect to city size, built-up surface area, and population, with shaded bars indicating the proportion of significant urbanization effects.

d Urbanization effects on HLP across Köppen–Geiger climate zones, including: tropical rainforest (Af), tropical monsoon (Am), tropical savannah (Aw), arid hot steppe (BSh), arid cold steppe (BSk), arid hot desert (BWh), arid cold desert (BWk), temperate with hot summer and no dry season (Cfa), temperate with warm summer and no dry season (Cfb), temperate with hot dry summer (Csa), temperate with warm dry summer (Csb), temperate with hot summer and dry winter (Cwa),

temperate with warm summer and dry winter (Cwb), cold with hot summer and no dry season (Dfa), cold with warm summer and no dry season (Dfb), and cold with hot summer and dry winter (Dwa). Boxplots show interquartile ranges (25th–75th percentiles), whiskers extend to non-outlier extremes, and medians are marked by horizontal lines. Outliers are shown as individual points. Gray numbers indicate valid city counts per zone. **e** Country-level urbanization effects (U_P , %) on HLP, with countries containing fewer than five selected cities marked in gray. The inserted number represents the number of cities used for analysis. Source data are provided as a Source Data file.

by enhanced light precipitation, while summer showed a more marked increase in heavy precipitation (16%). Regional contrasts were also evident, with urbanization effects differing in direction between seasons in regions such as the West Coast of the United States, Mediterranean Europe, and northern China.

Characteristics of urbanization effects

Our results demonstrate a general increase in lower-intensity precipitation and a decrease in higher-intensity events, leading to an overall reduction in HLP. However, strong spatial heterogeneity exists. To explore this variability, we assessed the relationship between urbanization effects on HLP and various urban, climatic, and geotopographic characteristics. We found that the proportion of cities showing reduced HLP increased with the degree of urbanization (Fig. 2a–c). Cities with larger size, greater built-up surface area, and higher population densities exhibited significantly higher proportions of HLP decline. Specifically, the proportions of significant HLP decreases in city groups with the largest size, surface area, and population (>90th quantile) are 6, 6, and 5 times as high as those in smaller cities (<10th quantile). A marked increase in the proportion of cities with significant HLP declines was observed above the 55th–65th percentile of urbanization, suggesting critical thresholds beyond which urban characteristics exert stronger influence on precipitation patterns. These thresholds correspond to cities with a total area between 219–271 km², built-up area of 48–62 km², and population ranging from 0.9 to 1.2 million. When urban attributes reach and exceed these critical ranges, the proportion of cities showing significant declines in HLP increases rapidly. Similar patterns can be found in the examinations for average city height and total building

volume (Supplementary Fig. 6a, b), highlighting a non-linear response of precipitation to urbanization.

In terms of climatic characteristics, cities in temperate zones consistently exhibited a negative urbanization effect on HLP (Fig. 2d). Notably, cities in the Cwb climate zone (temperate, dry winter, warm summer) showed the most pronounced decreases in HLP, with the most significant reductions in Mexico City (–56%). Weaker effects were observed in arid and cold regions, although cities in BWk (arid, desert, cold) and Dfb (cold, no dry season, warm summer) zones showed more complex patterns. Tropical cities in Af (rainforest) and Aw (savannah) climate zones generally exhibited reduced HLP, while cities in Am (monsoon) regions showed enhanced HLP. Geo-topographic factors, such as elevation and distance to the shoreline, did not show clear correlations with the impacts of urbanization on HLP (Supplementary Fig. 6c, d).

Finally, we provide a nationwide summarization, aiming to highlight countries experiencing the largest asymmetric shifts in precipitation distribution due to urbanization (Fig. 2e and Supplementary Fig. 7). To minimize the influence of extreme values (e.g., countries with only one examined city), we only considered countries with at least five study cities, resulting in a total of 30 countries examined here. Results show that for these 30 countries, 15 of them showed suppressed HLP smaller than –5% due to urbanization, while only Kazakhstan exhibited an increase (4%) in HLP. The countries with the largest reductions in HLP were Colombia (–20%), Australia (–19%), Nigeria (–16%), Argentina (–13%), and Japan (–12%). These findings highlight the urgent need for a reassessment of urban hydrological regimes on a national scale.

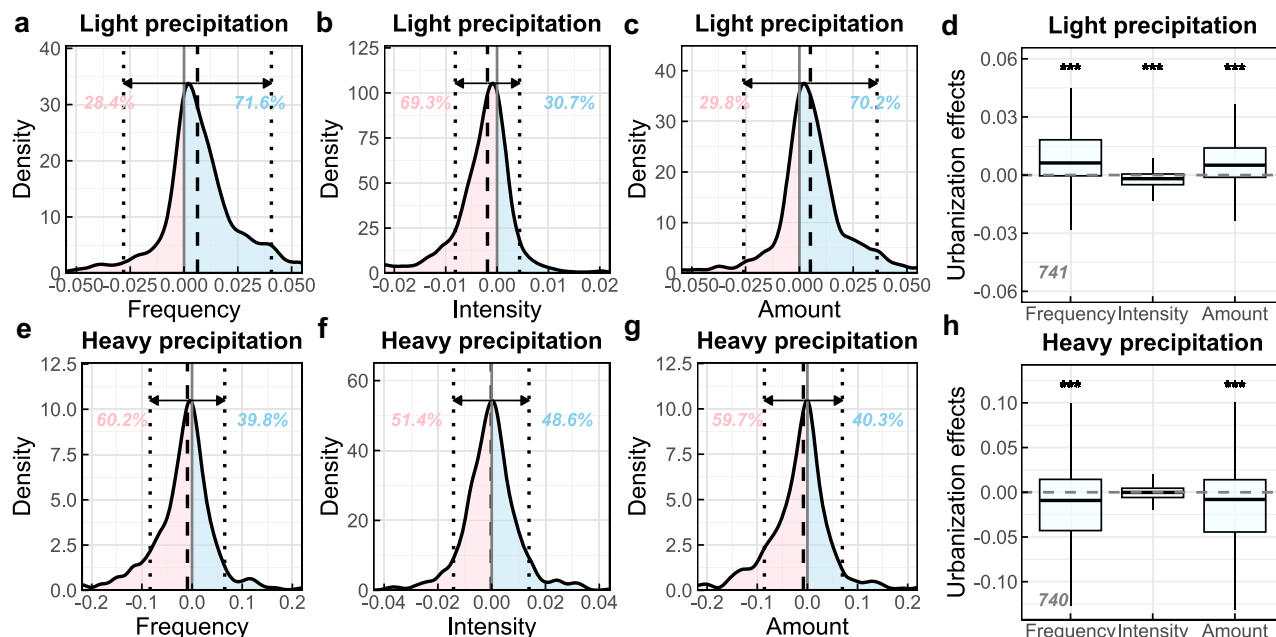


Fig. 3 | Partitioning of urbanization effects on precipitation. **a–c** Probability density distributions of urbanization effects on frequency, intensity, and amount for light precipitation. Vertical dashed and dotted lines indicate the median and ± 1 standard deviation, respectively. Blue and pink shaded areas represent positive (increase) and negative (decrease) effects, with colored numbers denoting the corresponding area under the curve. **d** Urbanization effects on partitioned components of light precipitation. Gray numbers indicate the number of cities

analyzed. Asterisks (***) denote statistically significant differences between urban and rural areas at the 99.9% confidence level. **e–g** Same as (a–c), but for heavy precipitation. **h** Same as (d), but for heavy precipitation. Note that the x-axis in (a–c, e–g) and the y-axis in (d, h) are logarithmic to partition changes in precipitation amount into frequency and intensity components (see “Methods”). Source data are provided as a Source Data file.

Partition of urbanization effects

Changes in the accumulated precipitation amount can be caused by either changes in precipitation frequency or intensity. To better understand changes in HLP, here we partitioned the urbanization effects on precipitation amount into frequency and intensity components. For light precipitation, 71.6% of cities showed increased frequency, while 69.3% exhibited reduced intensity, suggesting that increased frequency was the primary driver of higher accumulated light precipitation following urbanization (Fig. 3a–c). This is not surprising, as the intensity of light precipitation is restricted to a narrow range by definition (0.5–2.5 mm/h), so any changes in intensity could only exert limited impacts on the total amount (Fig. 3d). On average, urbanization increased light precipitation frequency by 1% while reducing intensity by 1% compared to rural areas (Supplementary Fig. 8a, b).

As for heavy precipitation, both frequency and intensity showed an overall decrease in urban areas compared to the surrounding rural regions (Fig. 3e–g). However, the reduction in heavy precipitation intensity is marginal, which is seen in 51.4% of cities with a slight reduction magnitude. In comparison, decreases in heavy precipitation frequency are found in around 60% of cities, with a mean decrease of 3%, which is primarily responsible for the observed decrease in heavy precipitation amount due to urbanization (Fig. 3h). Despite this overall trend, evident intensifications of both heavy precipitation frequency and intensity are observed in several coastal cities across different continents, such as Recife (Brazil), Fortaleza (Brazil), Houston (United States), and Chennai (India), potentially increasing flood risks there (Supplementary Fig. 8c, d).

Diurnal variability of urbanization effects

We subsequently analyzed the diurnal cycles of urbanization effects, focusing on light precipitation, heavy precipitation, and HLP. All three variables displayed similar diurnal cycles in both urban and rural areas,

suggesting that regional weather systems dominate the diurnal precipitation patterns. Averaged across all cities, the accumulated amount of light precipitation peaks in the afternoon (1500–1700 Local Solar Time (LST)) and reaches its lowest levels in the morning (0700–1000) (Fig. 4a). The diurnal cycle of heavy precipitation generally mirrors that of light precipitation but lags by 2–3 h, peaking in the late afternoon (1700–1900) and reaching its minimum around midday (1000–1300) (Fig. 4c). Additionally, heavy precipitation exhibits a secondary, albeit weaker, peak in the early morning (0500–0700). These cycles resulted in a bimodal HLP distribution, with one peak occurring in the early morning (0500–0700) and another in the late afternoon (1800–2000) (Fig. 4e).

The diurnal cycle of urbanization effects on light precipitation exhibited an inverse pattern compared to the diurnal cycle of light precipitation itself, with stronger positive effects in the early morning (0400–0800) and evening (2000–2200), and weaker effects around midday (1100–1500) (Fig. 4b). Similarly, the urbanization effect on heavy precipitation showed the strongest contrasts in the afternoon (1500–1800) and early morning (around 0600), with weaker effects at night (2000–0200) and midday (1000–1100) (Fig. 4d). Consequently, the urbanization effect on HLP displays two negative peaks (Fig. 4f). The early morning peak (0600) is driven by a combination of reduced heavy precipitation and enhanced light precipitation, while the afternoon peak (1500–1800) was primarily due to decreased heavy precipitation. The smallest urbanization effects on HLP occur around midday (1100–1400) when urbanization-induced changes in both light and heavy precipitation are relatively minor. Notably, the periods with larger negative urbanization-induced changes in HLP coincide with times of higher HLP values during the day, suggesting that urbanization tends to dampen the diurnal variability of HLP inherent in the regional weather system. Further analysis across different climate zones revealed broadly consistent diurnal behaviors, though with more

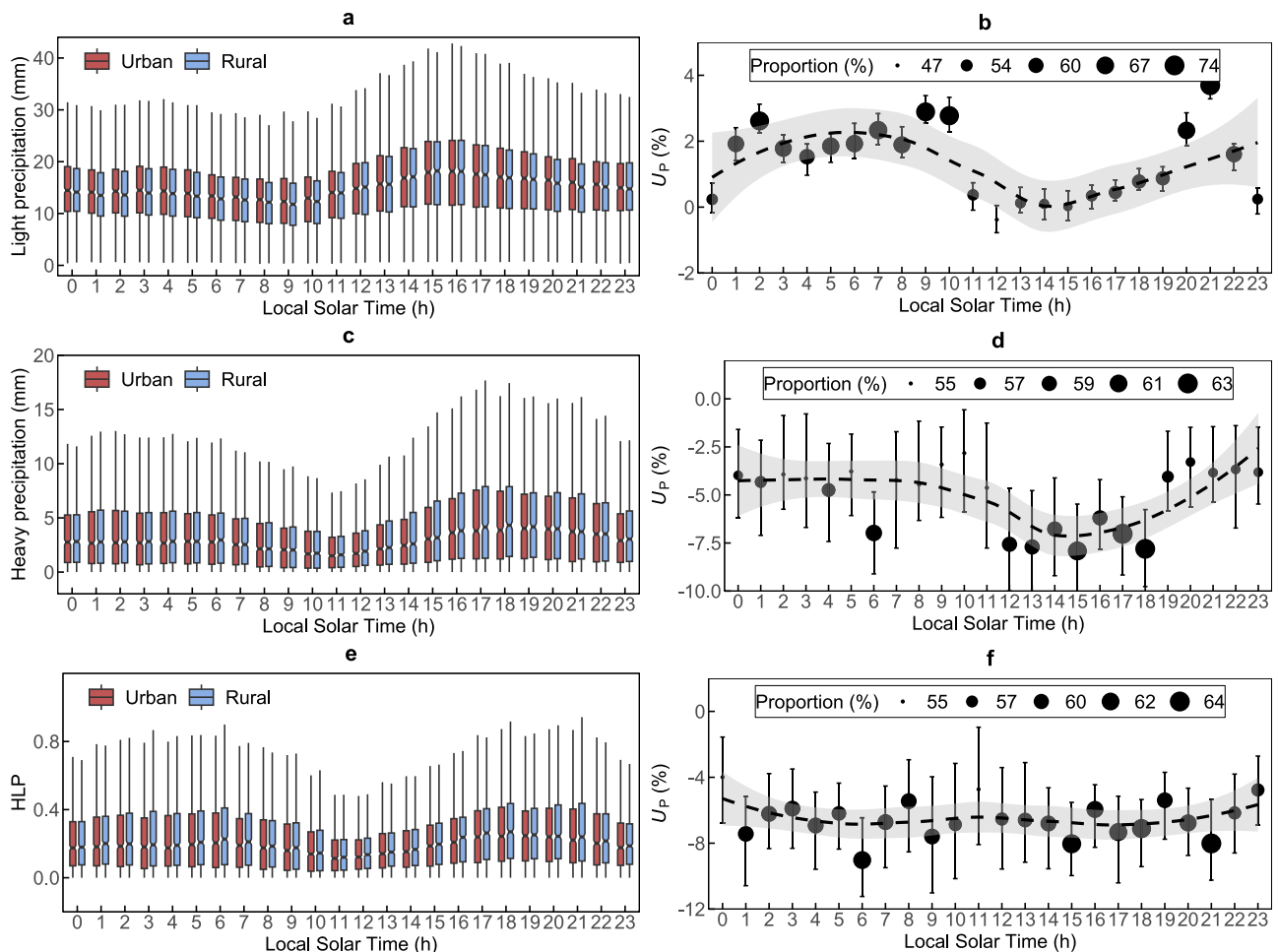


Fig. 4 | Diurnal variability of urbanization effects on precipitation. **a** Diurnal cycle of light precipitation over urban and rural regions. **b** Median urbanization effects (U_p , %) on light precipitation across global cities. Statistical significance is assessed using the non-parametric notch method at the 95% confidence level. Circle size indicates the proportion of cities with increased light precipitation; error bars represent uncertainty in the median estimated via a bootstrap method

($n=10,000$). The dashed line denotes the fitted diurnal cycle, with the gray shaded area indicating its 95% confidence interval. **c, d** Same as (**a, b**), but for heavy precipitation. In (**d**), circle size indicates the proportion of cities with decreased heavy precipitation. **e, f** Same as (**c, d**), but for the heavy-to-light precipitation ratio (HLP). In (**f**), circle size indicates the proportion of cities with decreased HLP. Source data are provided as a Source Data file.

pronounced sub-daily fluctuations in some regions (Supplementary Figs. 9–12).

Discussion

Widespread urbanization has profoundly altered regional atmospheric processes, reshaping precipitation patterns and complicating hydrological hazard mitigation in cities^{28,29}. However, quantifying the impact of urbanization on precipitation remains challenging due to the diversity of urban environments, the precipitation metrics used, the temporal scales considered, and the variety of data sources involved^{5,30}. Using a spatially continuous, high-resolution precipitation dataset, here we provide a pioneering global assessment of the impacts of urbanization on precipitation regimes, with a focus on shifts in the compositional distribution of precipitation intensities, offering insights into how urbanization reshapes precipitation characteristics and urban climate resilience.

Our findings reveal contrasting urbanization effects on different precipitation intensities, with a global tendency toward increased lower-intensity precipitation and decreased higher-intensity precipitation (Fig. 1b–d). These shifts suggest that urbanization generally acts to reduce the natural precipitation variability inherent in regional weather systems. Sub-daily analyses further show that light precipitation is primarily enhanced in the early morning, while heavy

precipitation is mostly suppressed in the late afternoon, indicating that urbanization dampens diurnal precipitation variability (Fig. 4b, d, f). These results are significant, as they imply that urbanization may mitigate warming-induced increases in precipitation variability under climate change in urban areas. However, this does not necessarily indicate a reduction in hydrological hazards, as changes in surface characteristics (e.g., infiltration capacity) could alter the response of surface hydrology to precipitation³¹. A coupled climate-hydrology analysis is needed to comprehensively assess the impacts of urbanization on hydrological hazards in cities.

Our finding that urbanization-induced precipitation increases are predominantly driven by enhancements in lower-intensity events contrasts somewhat with prior rain gauge-based studies, which have frequently highlighted elevated risks of heavy precipitation associated with urbanization effects^{20,32,33}. To evaluate the robustness of our results, we utilized NOAA's high-resolution (4 km) Analysis of Record for Calibration (AORC) regional precipitation dataset over the United States. Analyses employing AORC data generally supported the asymmetric precipitation responses identified in our primary analysis. Specifically, the F1 score³⁴—a predictive accuracy metric ranging from 0 (no skill) to 1 (perfect skill)—between AORC and IMERG was 0.55 for total precipitation anomalies, 0.77 for drizzle, and 0.64 for heavy precipitation across selected U.S. cities. Notably, performance

improved markedly in larger cities ($>1000 \text{ km}^2$), achieving F1 scores of 0.86 (total), 0.73 (drizzle), and 0.63 (heavy) (Supplementary Fig. 13).

Additionally, gauge-based studies often exhibit limited spatial representativeness, whereas satellite-derived precipitation datasets provide spatially comprehensive coverage, crucial for robust urban-rural comparative analyses. To illustrate this point, we conducted detailed case studies in China's three largest metropolitan areas—Beijing, Shanghai, and Guangzhou—each characterized by relatively dense gauge networks. We compared urbanization-induced precipitation signals obtained from gauges, IMERG grid cells co-located with gauge sites, and all IMERG grid cells across defined urban and rural domains. Significant discrepancies emerged between localized versus full IMERG domain estimates (Supplementary Fig. 14 and Supplementary Table 1). For example, in Shanghai, the urban-induced increase in low-intensity precipitation was estimated at 7.7% (local IMERG) and 6.5% (gauges), but declined sharply to 1.7% when considering all IMERG grid cells—a reduction likely due to the sparse distribution of rural gauges ($n = 3$). These findings underscore the inherent limitations of in-situ measurements, particularly in rapidly urbanizing and data-scarce regions, and emphasize the critical importance of satellite-based assessments with comprehensive spatial resolution in accurately capturing urbanization impacts on precipitation.

The observed changes in precipitation regimes may be linked to UHI effects through thermal and dynamic mechanisms^{35–37}. Rising temperatures disrupt boundary-layer stability, triggering regional circulations that enhance precipitation in inland and arid cities, where anthropogenic moisture sources amplify the urban wet island effect^{6,7,38,39}. This effect is more pronounced for light precipitation due to limited background moisture, which in turn suppresses heavy precipitation (Supplementary Fig. 15)⁴⁰. These dynamics are corroborated by significant positive (negative) correlations between UHI intensity and light (heavy) precipitation, contributing to widespread declines in HLP in arid and temperate zones (Fig. 1 and Supplementary Fig. 16a). In contrast, UHI effects intensify extreme precipitation in specific humid tropical cities (Fig. 1e)^{3,12}. This intensification is further amplified by the Clausius-Clapeyron relation stating an increased atmospheric moisture holding capacity as temperature rises (Supplementary Fig. 15b). However, such changes could in turn lead to decreases in available energy for producing light precipitation, as indicated by significant weaker/stronger negative correlations between UHI intensity and changes in heavy/light precipitation in tropical cities compared to other climates (Supplementary Fig. 16a). On a sub-daily scale, UHI effects intensify light precipitation at night (late evening and early morning), while reducing heavy precipitation during the day, especially in the late afternoon. This may be linked to cooling effects and reduced atmospheric moisture after light precipitation (Fig. 4d and Supplementary Fig. 16b, c). These findings highlight the significant role of thermal disturbances in altering regional precipitation regimes but also stress the complex interaction between urbanization and local climate conditions.

Beyond thermal mechanisms, urbanization also redistributes precipitation through dynamic and chemical processes⁴¹. Urban structures can fragment storm systems into smaller convective cells, increasing the frequency of low-intensity precipitation at the expense of high-intensity events^{42,43}. Enhanced surface roughness fosters vertical uplift and moisture convergence, further modulating precipitation patterns, as implied by the clear dependence of urbanization-induced HLP decrease on city size and build-up area (Fig. 2a, b)⁴⁴. Moreover, aerosol emissions exacerbate UHI effects by altering radiative balances, particularly through longwave absorption during nighttime, and act as cloud condensation nuclei, contributing to asymmetric precipitation changes⁴⁵. These mechanisms explain the spatial and diurnal variability in precipitation regime; however, the

magnitude and direction of changes remain uncertain, contingent on urban characteristics like size, shape, and morphology⁵.

Several limitations must be acknowledged. First, our analysis is based on urban-rural comparisons defined using the Global Urban Boundary (GUB) dataset⁴⁶. While dynamic buffering radii are used to account for spatial variability (Supplementary Fig. 1 and Eqs. 4 and 5), separating urbanization effects from natural variability (e.g., topography) and other human activities (e.g., irrigation) remains challenging. Second, the reliance on satellite-based precipitation products introduces uncertainties related to sensor calibration, retrieval errors, and orographic effects⁴⁷. Specifically, the spatial resolution of the IMERG dataset (0.1° , $\sim 10 \text{ km}$) may constrain its capacity to accurately capture localized, high-intensity precipitation events. To minimize the resolution limitation, we restrict our analysis to relatively larger cities with sizes greater than 100 km^2 . In addition, we assess against comprehensive ground observations in multiple aspects (Supplementary Figs. 17 and 18). Although comparisons with gauge data indicate a considerable underestimation of heavy precipitation in satellite products, this bias is consistent across both urban and rural areas, suggesting minimal impact on the assessment of urbanization effects on precipitation regimes. Additionally, we investigated the implications of spatial resolution limitations by utilizing the higher-resolution ($\sim 4 \text{ km}$) AORC dataset. Comparing native 4-km outputs with bilinearly interpolated 10-km datasets revealed only minor differences, with patterns qualitatively consistent with IMERG results (Supplementary Fig. 19). Consequently, resolution-induced biases appear minimal for cities larger than 100 km^2 . Nonetheless, future research should incorporate finer-scale regional high-resolution precipitation datasets, such as ground-based radar measurements and expanded gauge networks, to more precisely elucidate urbanization impacts on extreme precipitation events.

Methods

Selection of global cities

We initially identified 752 cities exceeding 100 km^2 worldwide using the GUB map⁴⁶. To ensure a clear distinction between urban and rural signals, cities whose designated rural buffers overlapped entirely with neighboring urban areas were excluded, resulting in a final set of 741 cities for analysis (Supplementary Fig. 7). The threshold of 100 km^2 was chosen to emphasize urbanization impacts in metropolitan regions, as smaller cities often exert limited influence on regional precipitation patterns³⁷. The selected cities are predominantly located in the Northern Hemisphere, with notable representation from the United States (209 cities) and China (129 cities). City boundaries were used to distinguish urban and rural precipitation estimates, generating 741 urban-rural pairs for comparative analysis (details in the next section).

The GUB dataset, spanning seven representative years (1990, 1995, 2000, 2005, 2010, 2015, and 2020), employs an automated framework integrating 30-meter global artificial impervious area data, which was derived from Landsat imagery, nighttime light data, and Sentinel-1 Synthetic Aperture Radar, achieving an overall accuracy exceeding 90%⁴⁸. Therefore, the GUB enables the extraction of the actual city boundary based on satellite images. The 2010 episode was selected to approximate average urbanization during the study period (2001–2023), emphasizing urban fringe areas through a morphological approach validated against Google Earth imagery and human interpretation. To assess the robustness of this choice, we compared results derived from the 2000 and 2020 urban boundaries and found no significant deviations from those based on the 2010 boundaries (details in the next section, Supplementary Figs. 20 and 21).

Delineation of city attributes

Urban characteristics for the selected cities, including surface area, height, and volume of artificial buildings, were derived from the Global Human Settlement Layer (GHSL, version R2023A) dataset at a 1 km

spatial resolution⁴⁹. The GHSL build-up surface area integrates data from advanced satellite imagers, including Landsat and Sentinel-2, with a global accuracy exceeding 90%. Note that its definition is different from city size, directly derived from GUB, instead focusing on the gross area of urban buildings within cities. Building heights were estimated using data from the ALOS Global Digital Surface Model (AW3D), NASA's Shuttle Radar Topographic Mission, and Sentinel-2 images⁵⁰. Building volumes were calculated using the corresponding estimates of surface area and height. Urbanization attributes were standardized to 2010, except for building height data, which was only available for 2018.

Several static geographic attributes that are likely relevant to regional precipitation patterns were also integrated, including elevation relief, climate classification, and distance to the shoreline. Elevation relief was determined using the HydroSHEDS digital elevation model at a 30 arc-second (~1 km) resolution⁵¹. Climate classifications were derived from the Köppen–Geiger system, based on the majority grid-cell type⁵². Shoreline distances were calculated as distances from city centroids to coastlines, based on the Global Self-consistent, Hierarchical, High-resolution Geography Database⁵³. These attributes were analyzed to evaluate spatial variations in urbanization effects.

Satellite precipitation product

Ground-based precipitation gauges always face limited spatial coverage, uneven distribution, and temporal discontinuity, making them insufficient for capturing global urbanization impacts on precipitation systems⁵⁴. To address this, we utilized gridded precipitation data from the Global Precipitation Measurement (GPM) project, an international satellite mission providing next-generation rain and snow observations, succeeding the Tropical Rainfall Measuring Mission⁵⁵. We employed the latest version of the Integrated Multi-satellite Retrievals for GPM (IMERG, Version 07B) algorithm, which intercalibrates, merges, and interpolates data from multiple passive microwave instruments and infrared sensors. The Final Run of IMERG was selected for its research-quality precipitation estimates during 2001–2023, offering a spatial resolution of 0.1° and a temporal resolution of 30 min, later aggregated to hourly scales⁵⁶. This resolution captures precipitation characteristics at the city level, with a median coverage of 12 urban and 13 rural grid cells per city pair (Supplementary Fig. 22). IMERG Version 07B includes advancements such as improved microwave inter-calibration, updated inputs, and enhanced precipitation rate caps, enabling more realistic extreme rainfall estimates compared to earlier versions. The IMERG dataset has been widely applied in detecting urbanization impacts on precipitation patterns globally^{12,57}.

We additionally evaluated another satellite-based precipitation product, the Global Satellite Mapping of Precipitation (GSMaP, Version 8)⁵⁸, which shares the same spatial and temporal resolution as IMERG. However, validation against extensive ground-based gauge observations revealed that IMERG consistently outperformed GSMaP in representing precipitation characteristics, especially for drizzle and heavy rainfall events (Supplementary Table 2). Furthermore, GSMaP did not effectively detect the expected urban rainfall island phenomenon globally (Supplementary Fig. 23), reinforcing our choice of IMERG as the primary dataset for analysis.

To substantiate our results, we also utilized the NOAA AORC dataset for urban areas in the United States. AORC is a high-resolution, multi-source precipitation product combining reanalysis data, in-situ observations, and satellite-derived estimates, and has been operational since 1979, serving as an essential input for National Water Model retrospective simulations⁵⁹. Comparative analyses between AORC and IMERG revealed consistent spatial distributions and minimal biases associated with the spatial resolution inherent to IMERG (Supplementary Figs. 13 and 19).

Gauge precipitation observations

To validate satellite data, we collected hourly precipitation records from the Global Sub-Daily Precipitation (GSDR) database, comprising 23,687 gauges subjected to rigorous quality control⁶⁰. Developed under the INTENSE project, the GSDR database aims to improve understanding of sub-daily precipitation extremes⁶¹. Additional hourly precipitation data from 2167 weather stations in China, verified by the China Meteorological Administration, were included⁶². Stations with less than 5 years of complete observations ($\geq 80\%$ completeness) and without overlap with GPM IMERG grid cells were excluded, resulting in 7288 stations worldwide (Supplementary Fig. 24). These include 1537 in China, 1089 in Japan, 973 in Germany, 1437 in the United Kingdom, and 1884 in the United States, aligning with regions where the selected cities are predominantly located.

We evaluated the percent bias (PBIAS, %) of total precipitation between gauge observations and GPM IMERG estimates (Supplementary Fig. 17). We found widespread overestimations of total precipitation from GPM IMERG across most countries, except for Finland and the United Kingdom, with median PBIAS values of 12.8% and 10% for urban and non-urban gauges, respectively. This overestimation may partially stem from missing gauge records or flagged abnormal observations excluded during data processing. Comparisons of light and heavy precipitation amounts (details in the next section) showed reasonable agreement between GPM IMERG and gauge data, despite a tendency for underestimation in heavy precipitation (Supplementary Fig. 18). This underestimation is likely due to scale mismatches between point-based gauge measurements and gridded satellite estimates, as well as potential limitations in the retrieval algorithms and associated parameterizations. Notably, these underestimations were consistent across both urban and rural areas, indicating minimal impact on the assessment of urbanization effects. It is also important to note that the IMERG algorithm does not incorporate land surface information in its precipitation retrievals. As a result, it is largely free from systematic artifacts introduced by urban surface characteristics, such as imperviousness or radiative anomalies. A recent independent evaluation further confirmed the capability of IMERG Version 07B in accurately capturing precipitation characteristics over urban regions⁶³. In addition, we conducted a performance comparison between IMERG and the GSMaP Version 8 product using gauge observations. Across multiple evaluation metrics, IMERG consistently outperformed GSMaP, particularly in capturing drizzle and heavy precipitation events. These results support the selection of IMERG as the primary dataset for our formal analysis (Supplementary Table 2).

Calculation of precipitation indices

This study examines the urban influence on the amount, distribution, and diurnal cycles of precipitation. First, we identified wet hours using a threshold of 0.1 mm/h, and calculated annual total precipitation as the sum of accumulated precipitation during all wet hours in a year. Precipitation intensities were categorized as drizzle (0.1–0.5 mm/h), light (0.5–2.5 mm/h), moderate (2.5–10 mm/h), and heavy (≥ 10 mm/h), based on the World Meteorological Organization's classification⁶⁴. We did not distinguish between liquid and solid precipitation (i.e., rain versus snow), as the vast majority of analyzed cities lie outside Arctic or high-latitude zones. Only one city in our study, La Paz (Bolivia), is classified as having a polar climate. Violent precipitation (≥ 50 mm/h) was merged with heavy events due to insufficient samples in arid cities. The use of a standard fixed threshold to categorize precipitation events facilitates consistent interpretation of urbanization influences across cities. Precipitation frequency was defined as the number of hours within a certain precipitation category, and the corresponding precipitation intensity was quantified using the simple precipitation

intensity index (I_i)⁶⁵:

$$I_i = \frac{A_i}{F_i} \quad (1)$$

where A_i is the total precipitation amount and F_i is the frequency for category i .

To evaluate changes in precipitation distribution, the HLP index was defined:

$$\text{HLP} = \frac{A_{\text{heavy precipitation}}}{A_{\text{light precipitation}}} \quad (2)$$

A higher HLP indicates a more variable precipitation distribution.

Diurnal precipitation indices were also calculated, with results transformed from Coordinated Universal Time (UTC) to LST as follows:

$$T_{\text{LST}}(h) = T_{\text{UTC}}(h) + \frac{\lambda(^{\circ})}{15(^{\circ} \cdot \text{h}^{-1})} \quad (3)$$

where λ represents longitude. Diurnal cycles were fitted using LOESS (locally estimated scatterplot smoothing) regression for clarity. All indices were computed for individual grid cells of the GPM IMERG product, followed by spatial integration at the city scale to represent urban precipitation characteristics.

Detection of urbanization influences

A paired method was employed to detect urbanization effects on regional climate, based on the assumption that urban and rural areas share comparable mesoscale atmospheric dynamics (e.g., convective system). Differences in precipitation patterns and related climate variables are thus attributed to contrasts in land surface properties, including urban-rural disparities and complex terrain. To account for the dynamic spatial extent of urbanization influences on precipitation, a buffer zone was established around each city with a radius (r) proportional to the city size (S):

$$r = \sqrt{\frac{S}{\pi}} \quad (4)$$

The urban area was defined as the region within this buffer, while the rural area was delineated between the second and third buffer zones ($2r$ to $3r$), with the intermediate zone ($1r$ to $2r$) serving as a transition area. Overlaps with rural zones from neighboring cities were excluded to avoid interference. Additionally, grid cells predominantly covered by water bodies (e.g., oceans or large lakes) were removed from both urban and rural domains using the 300-meter resolution GlobCover land cover map⁶⁶. This spatial delineation approach has been validated and widely adopted in previous global-scale studies of urbanization impacts on precipitation patterns^{12,67}. To test the sensitivity of our results to buffer size, we also experimented with a reduced buffer radius by applying a scaling coefficient to r (i.e., $(\sqrt{2} - 1) \cdot r$), ensuring more comparable spatial extents between urban and rural areas. However, this adjustment had negligible influence on our results (Supplementary Fig. 25), confirming the robustness of the adopted methodology⁶⁸.

Urban and rural regions were paired for analysis, resulting in 741 pairs worldwide. The relative urbanization effect on precipitation (U_p , %) was calculated as:

$$U_p = \frac{PI_{\text{urban}} - PI_{\text{rural}}}{PI_{\text{rural}}} \cdot 100\% \quad (5)$$

where PI represents the climatological status of precipitation indices during the study period. The relative format of U_p enables the

consideration of varying reference precipitation across different cities. Statistical significance ($p \leq 0.05$) was assessed using a t -test, with positive differences indicating enhancement and negative differences indicating suppression. The paired method was applied to each city individually, with multiple surrounding distances ($1r$ to $10r$) tested for robustness.

Partition of urbanization effects

To decompose urbanization-induced changes in precipitation amount, we partitioned these changes into frequency and intensity components using a logarithmic relationship⁶⁹:

$$\log A_{\text{urban}} - \log A_{\text{rural}} = (\log F_{\text{urban}} - \log F_{\text{rural}}) + (\log I_{\text{urban}} - \log I_{\text{rural}}) \quad (6)$$

Here, the logarithmic urbanization effects ($\log U_p$, dimensionless) on precipitation amounts reflect the combined influences of frequency and intensity. Statistical significance was tested as in U_p , and the probability density functions of urbanization effects on light and heavy precipitation (amount, frequency, and intensity) were estimated for probabilistic comparisons.

Quantification of urban heat island

To explore the linkage between UHI effects and precipitation changes, we calculated Spearman's rank correlation coefficient (r_s) between urbanization-induced precipitation effects (U_p) and UHI intensity. This non-parametric measure quantifies the association between rankings of the two variables. UHI intensity was derived as the contrast in average land surface temperature between the urban center and the rural area, which is defined as the first buffer zone surrounding the city. Diurnal cycles of UHI intensity were also analyzed to examine their relationship with sub-daily variations in precipitation. Temperature data was sourced from the global hourly, 5 km all-sky land surface temperature (GHA) dataset (2011–2023)⁷⁰. The GHA dataset, based on geostationary and polar-orbiting satellite data (e.g., CGLS, MODIS), employs a surface energy budget recovery method and has been extensively validated with ground measurements across diverse regions. Given the temporal overlap between GHA (2011–2023) and GPM IMERG, the r_s was calculated for this period to ensure consistency. This analysis provides insights into the physical mechanisms linking UHI effects and urbanization-induced precipitation changes.

Data availability

All the data supporting the main conclusion of this study can be freely accessed online. GPM IMERG data can be obtained from <https://gpm.nasa.gov/data/directory>, and the GPM-API tool can be used to download the data (<https://zenodo.org/records/13640487>). GSDR data can be obtained from <https://zenodo.org/records/8369987>. CMA data can be requested from the corresponding author. GUB data can be downloaded from <https://data-starcloud.pcl.ac.cn/>. The attributes of the cities can be extracted from: (1) HydroSHEDS, <https://www.hydrosheds.org/products/hydrosheds>; (2) GHSL, <https://human-settlement.emergency.copernicus.eu>; (3) GSHHG, <https://www.ngdc.noaa.gov/mgg/shorelines/shorelines.html>; (4) Global Köppen–Geiger climate classification map, <https://www.gloh2o.org/koppen/>. GHA data can be downloaded from <https://zenodo.org/records/7487284>. GlobCover data can be downloaded from <https://doi.org/10.1594/PANGAEA.787668>. Source data for generating Figs. 1–4 are provided with this paper. Source data are provided with this paper.

Code availability

The codes for calculating precipitation indices and producing main figures are available at Zenodo⁷¹.

References

- Zhao, M. et al. A global dataset of annual urban extents (1992–2020) from harmonized nighttime lights. *Earth Syst. Sci. Data* **14**, 517–534 (2022).
- Bazrkar, M. H., Zamani, N., Eslamian, S., Eslamian, A. & Dehghan, Z. Urbanization and Climate Change. In *Handbook of Climate Change Adaptation* (ed. Leal Filho, W.) 619–655 (Springer, 2015).
- Hao, L. et al. Urbanization alters atmospheric dryness through land evapotranspiration. *npj Clim. Atmos. Sci.* **6**, 1–10 (2023).
- Jabbar, H. K., Hamoodi, M. N. & Al-Hameedawi, A. N. Urban heat islands: a review of contributing factors, effects and data. *IOP Conf. Ser. Earth Environ. Sci.* **1129**, 012038 (2023).
- Liu, J. & Niyogi, D. Meta-analysis of urbanization impact on rainfall modification. *Sci. Rep.* **9**, 7301 (2019).
- Fan, Y., Li, Y., Bejan, A., Wang, Y. & Yang, X. Horizontal extent of the urban heat dome flow. *Sci. Rep.* **7**, 11681 (2017).
- Shem, W. & Shepherd, M. On the impact of urbanization on summertime thunderstorms in Atlanta: two numerical model case studies. *Atmos. Res.* **92**, 172–189 (2009).
- Miao, Y. et al. Simulating urban flow and dispersion in Beijing by coupling a CFD model with the WRF model. *Adv. Atmos. Sci.* **30**, 1663–1678 (2013).
- Fan, J., Zhang, Y., Li, Z., Hu, J. & Rosenfeld, D. Urbanization-induced land and aerosol impacts on sea-breeze circulation and convective precipitation. *Atmos. Chem. Phys.* **20**, 14163–14182 (2020).
- Lin, Y. et al. Urbanization-induced land and aerosol impacts on storm propagation and hail characteristics. *J. Atmos. Sci.* **78**, 925–947 (2021).
- Qian, Y. et al. Urbanization impact on regional climate and extreme weather: current understanding, uncertainties, and future research directions. *Adv. Atmos. Sci.* **39**, 819–860 (2022).
- Sui, X., Yang, Z.-L., Shepherd, M. & Niyogi, D. Global scale assessment of urban precipitation anomalies. *Proc. Natl. Acad. Sci. USA* **121**, e2311496121 (2024).
- Huang, X. et al. Influence of urbanization on hourly extreme precipitation over China. *Environ. Res. Lett.* **17**, 044010 (2022).
- Singh, J., Karmakar, S., PaiMazumder, D., Ghosh, S. & Niyogi, D. Urbanization alters rainfall extremes over the contiguous United States. *Environ. Res. Lett.* **15**, 074033 (2020).
- Song, X. et al. Impacts of urbanization on precipitation patterns in the greater Beijing–Tianjin–Hebei metropolitan region in northern China. *Environ. Res. Lett.* **16**, 014042 (2021).
- Tysa, S. K. & Ren, G. Observed decrease in light precipitation in part due to urbanization. *Sci. Rep.* **12**, 3864 (2022).
- Wu, L., Ye, A., Wang, Y., Li, Q. & Zhan, S. Urbanization influence on changes of extreme precipitation in mainland China. *Glob. Planet. Change* **246**, 104720 (2025).
- Li, F. et al. Assessing the consistent and divergent impacts of urbanization on heavy rainfall in Chinese urban agglomerations. *Commun. Earth Environ.* **6**, 1–12 (2025).
- Huang, S. et al. Urbanization amplified asymmetrical changes of rainfall and exacerbated drought: analysis over five urban agglomerations in the Yangtze River Basin, China. *Earth's Future* **11**, e2022EF003117 (2023).
- Yu, X. et al. Asymmetrical shift toward less light and more heavy precipitation in an urban agglomeration of East China: intensification by urbanization. *Geophys. Res. Lett.* **49**, e2021GL097046 (2022).
- Li, F. et al. Does urbanization exacerbate asymmetrical changes in precipitation at divergent time scales in China? *Earth's Future* **12**, e2023EF004355 (2024).
- Knapp, A. K. et al. Consequences of more extreme precipitation regimes for terrestrial ecosystems. *Bioscience* **58**, 811–821 (2008).
- Dunkerley, D. L. Light and low-intensity rainfalls: a review of their classification, occurrence, and importance in landsurface, ecological and environmental processes. *Earth Sci. Rev.* **214**, 103529 (2021).
- Wu, M., Luo, Y., Chen, F. & Wong, W. K. Observed link of extreme hourly precipitation changes to urbanization over coastal South China. *J. Appl. Meteorol. Climatol.* **58**, 1799–1819 (2019).
- Fu, X., Yang, X.-Q. & Sun, X. Spatial and diurnal variations of summer hourly rainfall over three super city clusters in Eastern China and their possible link to the urbanization. *J. Geophys. Res. Atmos.* **124**, 5445–5462 (2019).
- Zhu, X. et al. Impact of urbanization on hourly precipitation in Beijing, China: spatiotemporal patterns and causes. *Glob. Planet. Change* **172**, 307–324 (2019).
- Yang, T., Lu, X., Xiang, K., Jiang, M. & Qiu, Y. Variation characteristics and the influences of urbanization on hourly intense precipitation before and after monsoon onset over the Pearl River Delta. *Sci. Rep.* **14**, 26864 (2024).
- Vo, T. T., Hu, L., Xue, L., Li, Q. & Chen, S. Urban effects on local cloud patterns. *Proc. Natl. Acad. Sci. USA* **120**, e2216765120 (2023).
- Georgescu, M., Broadbent, A. M. & Krayenhoff, E. S. Quantifying the decrease in heat exposure through adaptation and mitigation in twenty-first-century US cities. *Nat. Cities* **1**, 42–50 (2024).
- Lalonde, M., Oudin, L. & Bastin, S. Urban effects on precipitation: Do the diversity of research strategies and urban characteristics preclude general conclusions? *Urban Clim.* **51**, 101605 (2023).
- Balaian, S. K., Sanders, B. F. & Abdolhosseini Qomi, M. J. How urban form impacts flooding. *Nat. Commun.* **15**, 6911 (2024).
- Tysa, S. K. & Ren, G. Urbanization signal in long-term precipitation trends estimated based on observed data of national meteorological stations over China Mainland. *J. Clim.* **38**, 2225–2238 (2025).
- Tysa, S. K., Ren, G., Zhang, P. & Zhang, S. Impact of urbanization on regional extreme precipitation trends observed at China national station network. *Weather Clim. Extrem.* **48**, 100760 (2025).
- Christen, P., Hand, D. J. & Kirielle, N. A review of the F-measure: its history, properties, criticism, and alternatives. *ACM Comput. Surv.* **56**, 1–24 (2023).
- Shepherd, J. M. A review of current investigations of urban-induced rainfall and recommendations for the future. *Earth Interact.* **9**, 1–27 (2005).
- Oke, T. R. City size and the urban heat island. *Atmos. Environ.* **7**, 769–779 (1973).
- Georgescu, M., Broadbent, A. M., Wang, M., Krayenhoff, E. S. & Moustauoi, M. Precipitation response to climate change and urban development over the continental United States. *Environ. Res. Lett.* **16**, 044001 (2021).
- Huang, X. & Song, J. Urban moisture and dry islands: spatio-temporal variation patterns and mechanisms of urban air humidity changes across the globe. *Environ. Res. Lett.* **18**, 103003 (2023).
- Luo, Z. et al. Seasonal variation of dry and wet islands in Beijing considering urban artificial water dissipation. *npj Clim. Atmos. Sci.* **4**, 1–9 (2021).
- Meyer, J., Neuper, M., Mathias, L., Zehe, E. & Pfister, L. Atmospheric conditions favouring extreme precipitation and flash floods in temperate regions of Europe. *Hydrol. Earth Syst. Sci.* **26**, 6163–6183 (2022).
- Zhang, D.-L. Rapid urbanization and more extreme rainfall events. *Sci. Bull.* **65**, 516–518 (2020).
- Miao, S., Chen, F., Li, Q. & Fan, S. Impacts of urban processes and urbanization on summer precipitation: a case study of heavy rainfall in Beijing on 1 August 2006. *J. Appl. Meteorol. Climatol.* **50**, 806–825 (2011).

43. Niyogi, D. et al. Urban modification of thunderstorms: an observational storm climatology and model case study for the Indianapolis urban region. *J. Appl. Meteorol. Climatol.* **50**, 1129–1144 (2011).
44. Li, Y. et al. Strong intensification of hourly rainfall extremes by urbanization. *Geophys. Res. Lett.* **47**, e2020GL088758 (2020).
45. Cao, C. et al. Urban heat islands in China enhanced by haze pollution. *Nat. Commun.* **7**, 12509 (2016).
46. Li, X. et al. Mapping global urban boundaries from the global artificial impervious area (GAIA) data. *Environ. Res. Lett.* **15**, 094044 (2020).
47. Tian, Y. et al. Component analysis of errors in satellite-based precipitation estimates. *J. Geophys. Res. Atmos.* **114**, D24101 (2009).
48. Gong, P. et al. Annual maps of global artificial impervious area (GAIA) between 1985 and 2018. *Remote Sens. Environ.* **236**, 111510 (2020).
49. Pesaresi, M. & Politis, P. GHS-BUILT-S R2023A - GHS built-up surface grid, derived from Sentinel2 composite and Landsat, multitemporal (1975–2030). European Commission, Joint Research Centre (JRC). Accessed 6 June 2025, <http://data.europa.eu/89h/9f06f36f-4b11-47ec-abb0-4f8b7b1d72ea> (2023).
50. Pesaresi, M. et al. Advances on the Global Human Settlement layer by joint assessment of Earth observation and population survey data. *Int. J. Digit. Earth* **17**, 2404284 (2024).
51. Lehner, B., Verdin, K. & Jarvis, A. New global hydrography derived from spaceborne elevation data. *Eos Trans. Am. Geophys. Union* **89**, 93–94 (2008).
52. Beck, H. E. et al. Present and future Köppen-Geiger climate classification maps at 1-km resolution. *Sci. Data* **5**, 180214 (2018).
53. Wessel, P. & Smith, W. H. F. A global, self-consistent, hierarchical, high-resolution shoreline database. *J. Geophys. Res. Solid Earth* **101**, 8741–8743 (1996).
54. Kidd, C. et al. So, How much of the Earth's surface is covered by rain gauges? *Bull. Am. Meteorol. Soc.* **98**, 69–78 (2017).
55. Skofronick-Jackson, G. et al. The Global Precipitation Measurement (GPM) mission for science and society. *Bull. Am. Meteorol. Soc.* **98**, 1679–1695 (2017).
56. Huffman et al. IMERG V07 Release Notes. Accessed 6 June 2025, <https://gpm.nasa.gov/resources/documents/imerg-v07-release-notes> (2024).
57. Yang, L. et al. Urban development pattern's influence on extreme rainfall occurrences. *Nat. Commun.* **15**, 3997 (2024).
58. Kubota, T. et al. Global Satellite Mapping of Precipitation (GSMaP) Products in the GPM Era. In *Satellite Precipitation Measurement Vol. 1* (ed. Levizzani, V. et al.) 355–373 (Springer International Publishing, 2020).
59. Fall, G. et al. The Office of Water Prediction's Analysis of Record for Calibration, version 1.1: dataset description and precipitation evaluation. *J. Am. Water Resour. Assoc.* **59**, 1246–1272 (2023).
60. Lewis, E. et al. GSDR: a global sub-daily rainfall dataset. *J. Clim.* **32**, 4715–4729 (2019).
61. Blenkinsop, S. et al. The INTENSE project: using observations and models to understand the past, present and future of sub-daily rainfall extremes. in *Advances in Science and Research* Vol. 15, 117–126 (Copernicus GmbH, 2018).
62. Ren et al. Quality control procedures for hourly precipitation data from automatic weather stations in China. *Meteorol. Mon.* **36**, 123–132 (2010).
63. Xiong, J., Tang, G. & Yang, Y. Continental evaluation of GPM IMERG V07B precipitation on a sub-daily scale. *Remote Sens. Environ.* **321**, 114690 (2025).
64. World Meteorological Organization (WMO). *Guide to Instruments and Methods of Observation* (WMO-No. 8) Accessed 6 June 2025, <https://library.wmo.int/idurl/4/41650> (2021–2023).
65. Karl, T. R., Nicholls, N. & Ghazi, A. CLIVAR/GCOS/WMO Workshop on Indices and Indicators for Climate Extremes Workshop Summary. in *Weather and Climate Extremes: Changes, Variations and a Perspective from the Insurance Industry* (eds Karl, T. R., Nicholls, N. & Ghazi, A.) 3–7 (Springer Netherlands, 1999).
66. Arino, O. et al. Global Land Cover Map for 2009 (GlobCover 2009). © European Space Agency (ESA) & Université catholique de Louvain (UCL) PANGAEA. Accessed 6 June 2025, <https://doi.org/10.1594/PANGAEA.787668> (2012).
67. Huang, S. et al. Widespread global exacerbation of extreme drought induced by urbanization. *Nat. Cities* **1**, 1–13 (2024).
68. Zhang, L. et al. Direct and indirect impacts of urbanization on vegetation growth across the world's cities. *Sci. Adv.* **8**, eabo0095 (2022).
69. Xiong, J. et al. Variation and attribution of probable maximum precipitation of China using a high-resolution dataset in a changing climate. *Hydrol. Earth Syst. Sci.* **28**, 1873–1895 (2024).
70. Jia, A. et al. Global hourly, 5 km, all-sky land surface temperature data from 2011 to 2021 based on integrating geostationary and polar-orbiting satellite data. *Earth Syst. Sci. Data* **15**, 869–895 (2023).
71. Xiong, J. Asymmetric shifts in precipitation due to urbanization across global cities. Zenodo, Accessed 6 June 2025, <https://zenodo.org/records/8423726> (2025).

Acknowledgements

This study was financially supported by the Ministry of Science and Technology of China [Grant No. 2023YFC3206603 (Y.Y.) and 2023YFC3006702 (Y.Y.)], the Science and Technology Department of Qinghai Province [Grant No. 2024-SF-A6 (Y.Y.)], and the Basic Research Program of Jiangsu Province [Grant No. BK20231541 (Y.L.)]. We thank Zifeng Deng from Princeton University for the interactive discussion.

Author contributions

J.X., Y.Y., and D.Y. initiated the idea and designed the study. J.X. and Y.Y. performed the analyses and drafted the manuscript. L.Y. contributed to the results discussion and the review and editing of the manuscript. Y.Y. acquired funding for this research.

Competing interests

The authors declare no competing interests.

Additional information

Supplementary information The online version contains supplementary material available at <https://doi.org/10.1038/s41467-025-61053-0>.

Correspondence and requests for materials should be addressed to Yuting Yang or Dawen Yang.

Peer review information *Nature Communications* thanks Lindsey Hayden, Manmeet Singh, and Xiaomeng Song for their contribution to the peer review of this work. A peer review file is available.

Reprints and permissions information is available at <http://www.nature.com/reprints>

Publisher's note Springer Nature remains neutral with regard to jurisdictional claims in published maps and institutional affiliations.

Open Access This article is licensed under a Creative Commons Attribution-NonCommercial-NoDerivatives 4.0 International License, which permits any non-commercial use, sharing, distribution and reproduction in any medium or format, as long as you give appropriate credit to the original author(s) and the source, provide a link to the Creative Commons licence, and indicate if you modified the licensed material. You do not have permission under this licence to share adapted material derived from this article or parts of it. The images or other third party material in this article are included in the article's Creative Commons licence, unless indicated otherwise in a credit line to the material. If material is not included in the article's Creative Commons licence and your intended use is not permitted by statutory regulation or exceeds the permitted use, you will need to obtain permission directly from the copyright holder. To view a copy of this licence, visit <http://creativecommons.org/licenses/by-nc-nd/4.0/>.

© The Author(s) 2025